Evidence of austenite by-passing in a stainless steel obtained from laser melting additive manufacturing

Michella Alnajjar, Frédéric Christien, Krzysztof Wolski, Cedric Bosch

Evidence of austenite by-passing in a stainless steel obtained from laser melting additive manufacturing

Michella Alnajjar[a], Frédéric Christien[a], Krzysztof Wolski[a], Cedric Bosch[a]

[a] Mines Saint-Etienne, Univ Lyon, CNRS, UMR 5307 LGF, Centre SMS, F - 42023 Saint-Etienne France

Microstructural characterization was carried out on AISI 17-4 PH stainless steel fabricated by selective laser melting (SLM) in an argon environment. Conventionally, this steel exhibits a martensitic structure with a small fraction of δ ferrite. However, the combined findings of x-ray diffraction and electron backscatter diffraction (EBSD) proved that SLM-ed 17-4 PH steel has a fully ferritic microstructure, more specifically δ ferrite. The microstructure consists of coarse ferritic grains elongated along the build direction, with a pronounced solidification crystallographic texture. These results were associated to the high cooling and heating rates experienced throughout the SLM process that suppressed the austenite formation and produced a "by-passing" phenomenon of this phase during the numerous thermal cycles. Furthermore, the energy-dispersive X-ray spectroscopy (EDS) measurements revealed a uniform distribution of elements without any dendritic structure. The extremely high cooling kinetics induced a diffusionless solidification, resulting in a homogeneous elemental composition. It was also found that the ferritic SLM-ed material can be transformed to martensite again by re-austenitization at 1050°C followed by quenching.

Keywords: stainless steel, martensite, ferrite, selective laser melting, phase transformation

1. Introduction

Additive manufacturing (AM) has been rapidly developing in the past few years, because it allows 3D parts, often having a complex geometry, to be directly fabricated to a near-net-shape. It consists of constructing a

part by adding materials layer upon layer according to a CAD (Computer-aided design) model. In contrast to conventional “subtractive” methods, it requires little machining and finishing work, thus reducing waste to a minimum. AM refers to the process itself which incorporates several techniques [1–3]. One of these techniques is selective laser melting (SLM) that is based on powder bed fusion. Atomized metal powder are deposited on a substrate plate and selectively melted by a laser beam using CAD data. Subsequently, the building platform is lowered and another powder layer is re-deposited. The procedure repeats itself until reaching the required shape. Numerous construction parameters such as laser power and speed, scanning strategy and build chamber atmosphere, should be controlled in order to obtain a nearly fully dense functioning part [4–7]. Although this technology has progressed greatly, there are still various limitations. Among them can be cited: the limited material that can be used, poor surface quality and the resulting non-equilibrium microstructures. In addition, many reports revealed that some alloys processed by SLM presented highly anisotropic microstructures [8,9] that are sometimes greatly different from those obtained by conventional fabrication routes.

This study focuses on the microstructure of 17-4 PH stainless steel fabricated by SLM process. Wrought 17-4 PH steel is a martensitic precipitation hardenable stainless steel. It is widely used in a variety of applications such as aerospace, medical and food industries, due to its high strength and relatively good corrosion resistance. A solution heat treatment is usually applied in the austenitic domain (~1050°C), followed by quenching, to obtain a martensitic structure. In order to improve the mechanical properties, a subsequent tempering treatment in the range 480°-620°C is conducted that results in precipitation-hardening by copper precipitates [10–12]. Recent studies on this steel fabricated by SLM method have investigated the effect of multiple process parameters on material properties. According to Z. Hu et al. [13], the scan velocity and layer thickness were the key factors in controlling the material density at a fixed laser power. An interaction between these factors was also taken into account. Moreover, the building orientation had a great effect on mechanical properties. A. Yadollahi et al. found that the horizontal building orientation was more favorable because it allowed fewer defects to be formed by decreasing the number of deposited layers [14,15]. In addition, a change in phase constitution was reported by multiple authors that strongly depended on the chamber atmosphere. For instance, a significant fraction of retained austenite was found in this material when built in a chamber with nitrogen atmosphere, while in an argon purging environment, the microstructure was identified as mainly

martensitic. It was deduced that the nitrogen had a strong stabilizing effect on the austenitic phase [16–19]. Moreover, besides the highly anisotropic and textured microstructure usually found in these materials, some investigations have revealed a dendritic/cellular structure with micro-segregation. It was attributed to the high cooling rates (10^5-10^6 K/s) experienced during SLM that led to non-equilibrium solidification conditions [18,19].

The existing literature on SLM-ed 17-4 PH steel mainly focused on the effect of process parameters on the resulting microstructures, especially the retained austenite. However, little attention was paid on this SLM-ed steel when having a fully body centered cubic structure. In this present work, a detailed microstructural characterization was conducted on SLM-ed 17-4 PH steel fabricated under argon atmosphere.

2. Experimental procedure

Microstructural analysis was carried out on both wrought and SLM-ed 17-4 PH stainless steel. The wrought material is commercial 17-4 PH steel from UGINE (cast # 818025). Parts were cut from a 15 mm diameter wrought rod bar. They were heat treated at 1050°C for an hour followed by water quenching, which led to a martensitic structure. The main study of SLM-ed material was done on a specimen having a cuboidal shape with dimensions 12x12x60 mm. It was fabricated using a selective laser melting machine (SLM 280 solution) under an argon purging atmosphere. Laser was operating at a power of 275 W and a scanning speed of 760 mm/s. The powder layer thickness was approximately 50 µm and a scanning strategy of stripes was applied with a 90° rotation between layers. The build orientation was horizontal, meaning that the longitudinal axis of the cuboid was horizontal and parallel to the build platform (X-Y plane). Parts were cut from the specimen parallel (Y-Z plane) and perpendicular (X-Y plane) to the build direction Z. A schematic representation of the cuboid and its corresponding studied planes is given in Fig. 1. Note that the SLM-ed samples were studied both in the as-built condition and after a solution heat treatment (1050°C/1 hour + water quench). The chemical compositions for both wrought and SLM-ed 17-4 PH are given in table 1. For wrought material, the full composition of the cast is indicated (data from the steel provider) in the first line of table 1. Additional measurements were conducted in this study on both wrought and SLM-ed materials (lines 2 and 3 of table 1). These measurements were carried out using X-ray fluorescence (XRF) (FISCHERSCOPE X-Ray XAN-FD) for elements Ni, Cr and Cu, and using combustion elemental analysis (CEA) for C, S (LECO CS 444/LS), N and O (LECO TC-436).

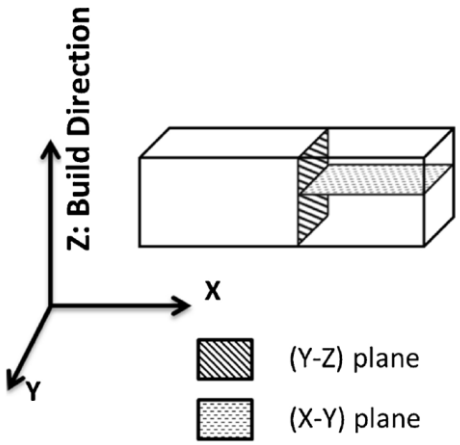

Figure 1: Schematic representation of the build orientation and the planes at which the microstructural characterization was carried out.

Phase identification was conducted in PANalytical's X'Pert PRO X-ray diffractometer using Cu kα radiation. X-ray diffraction patterns were obtained within 2Θ range of 40° to 120° at a step size of 0.04°. For optical microscopy, samples were polished to a mirror finish, and then etched with a modified Villela reagent (10 g picric acid+ 10 ml hydrochloric acid+ 8 ml acetic acid+ 100 ml ethanol) for 30 s to reveal the martensitic microstructures. An electrochemical etching was also applied using concentrated nitric acid solution (50% HNO_3) at 2 V for 20 s to reveal the austenitic grain boundaries. Regarding scanning electron microscopy (SEM) preparation, samples were polished up to 1200 grit, followed by electropolishing using 94% ethanol + 6% perchloric acid as electrolyte at 25 V for 60 s. SEM Zeiss SUPRA55VP was used for microstructural observations in electron backscatter diffraction (EBSD) mode operating at 20 kV. In addition, microchemical analysis was performed using energy dispersive spectroscopy (EDS). Dilatometric testing was carried out in a SETARAM dilatometer under an argon atmosphere, while continuous heating and cooling were maintained at a fixed rate of 5 K/min.

In order to ensure reproducibility, two other SLM-ed samples were studied by using EBSD and EDS techniques. They were fabricated in different machines (Machine 1: SLM solution 280 HL, machine 2: Concept Laser M2) but had the same atmosphere (argon) in the building chamber similar to that used for the main SLM-ed specimen.

Table 1: Chemical composition (wt. %) of wrought and SLM-ed 17-4 PH stainless steel

17-4 PH		C	Ni	Si	P	Mn	Cr	Cu	S	N	O	Nb	Fe
Wrought	Provider Data sheet	0.031	4.82	0.31	0.016	0.81	15.61	3.12	0.02	-	-	0.21	Bal.
	XRF/CEA	0.026	4.95	-	-	-	16.18	3.09	0.021	0.033	0.007	-	Bal.
SLM-ed	XRF/CEA	0.011	3.98	-	-	-	15.87	3.63	0.005	0.058	0.070	0.57	Bal.

3. Results and discussion

3.1. Microstructure of wrought 17-4 PH steel

The optical observation of wrought 17-4 PH steel revealed a typical lath martensite structure inside well defined prior austenitic grains as shown in Fig. 2(a). The average size of the austenitic grains is approximately 18 µm. The inverse pole figure IPF map in Fig. 2(b) shows the lathes of martensite grouped into different packets inside the same prior austenite grain. These packets are separated by grain boundaries having misorientation angles higher than 10°. As expected, the material has undergone a complete martensitic transformation upon quenching after a heat treatment at 1050°C.

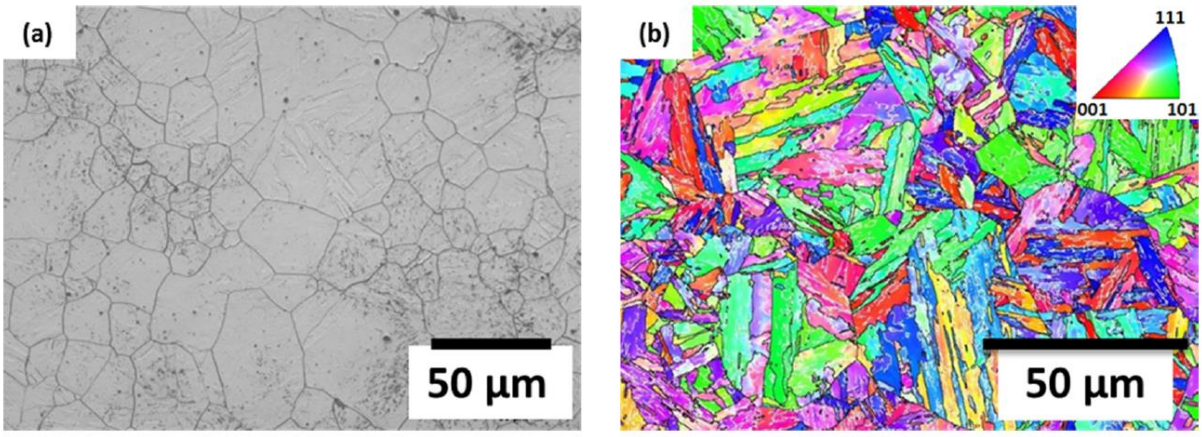

Figure 2: (a) Optical micrograph and (b) EBSD orientation map (IPF Z) of wrought 17-4 PH steel showing a typical martensitic microstructure with a mean grain size of 18 µm.

3.2. Phase identification in as-built 17-4 PH steel

Fig. 3(a) and (b) show respectively the XRD diffraction patterns obtained from the planes (Y-Z) (parallel to the build direction) and (X-Y) (perpendicular to the build direction) for the as-built sample. It can be seen that in both planes the structure consists almost entirely of BCC phase with a small fraction of FCC austenite. The austenitic content is estimated to be less than 5%. It should be noted that the BCC phase can be attributed to either the martensite or ferrite, since the two phases cannot be distinguished by the XRD method. The martensite in stainless steels with a carbon content less than 0.2%, which is the case of 17-4 PH steel, has a BCC structure just as ferrite. Only for carbon content higher than 0.2% the martensite becomes slightly quadratic [20]. Furthermore, the peak intensity differences between the two planes (Y-Z) and (X-Y) show that the material is crystallographically textured.

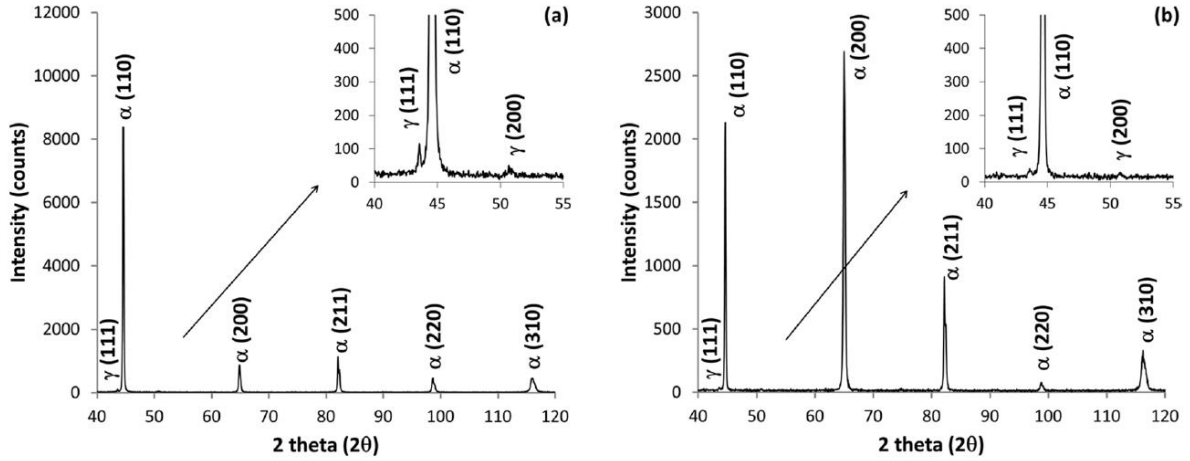

Figure 3: XRD patterns of as-built 17-4 PH steel (a) in the (Y-Z) plane parallel to the build direction and (b) in the (X-Y) plane perpendicular to the build direction.

3.3. Microstructure of as-built 17-4 PH steel

The optical micrographs and EBSD orientation maps of the as-built 17-4 PH sample in the planes (Y-Z) and (X-Y) are shown respectively in fig. 4 and 5. Both planes reveal a coarse grain microstructure with no presence of

lathes of martensite or any other large misorientations within the grains, characteristics for this type of microstructure. The as-built 17-4 PH steel observed here doesn't have a martensitic structure. This contradicts with the existing literature [14,16,18] where the authors had the same observations (optical and EBSD) of the SLM-ed 17-4 PH steel fabricated in an argon environment, but they considered the BCC phase to be martensite. As demonstrated using X-ray diffraction earlier (par. 3.2), this material consists mainly of a BCC phase which could either be martensite or ferrite. Thus the combined XRD and EBSD observations directly imply that this material has a fully ferritic BCC microstructure. In a similar manner, some studies reported a fully ferritic microstructure of duplex stainless steels in the as-built condition compared with their conventional dual phase structure (ferrite + austenite) [21,22]. This shows that the austenite by-passing effect observed here is also possible on other types of steels.

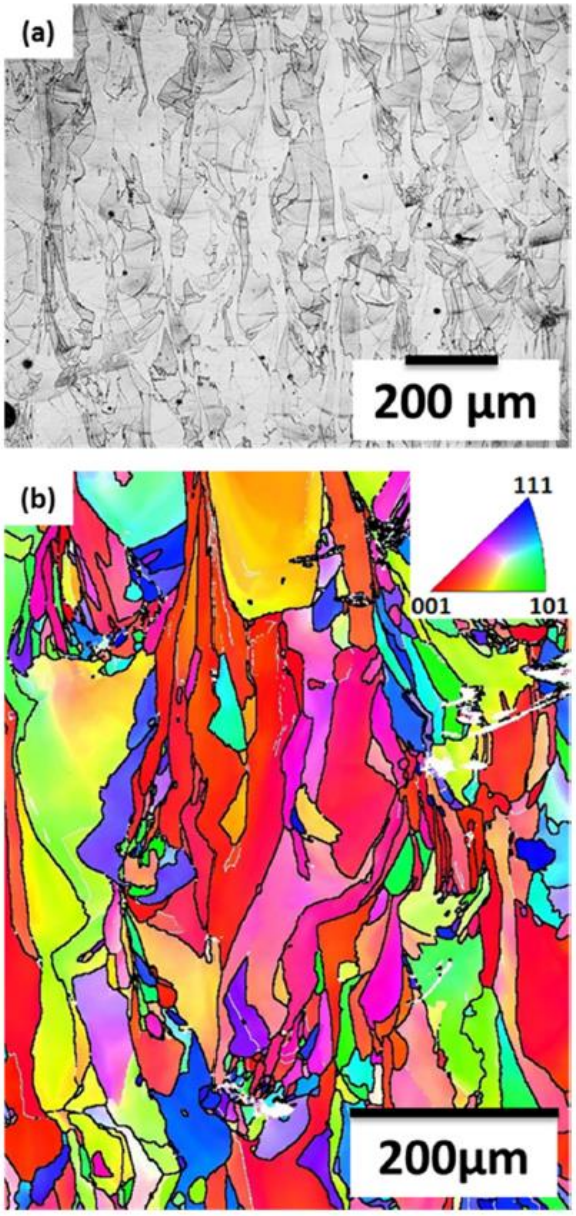

Figure 4: (a) Optical micrograph and (b) EBSD orientation map (IPF Z) of as-built 17-4 PH steel in the (Y-Z) plane showing coarse grains with epitaxial growth in the build direction.

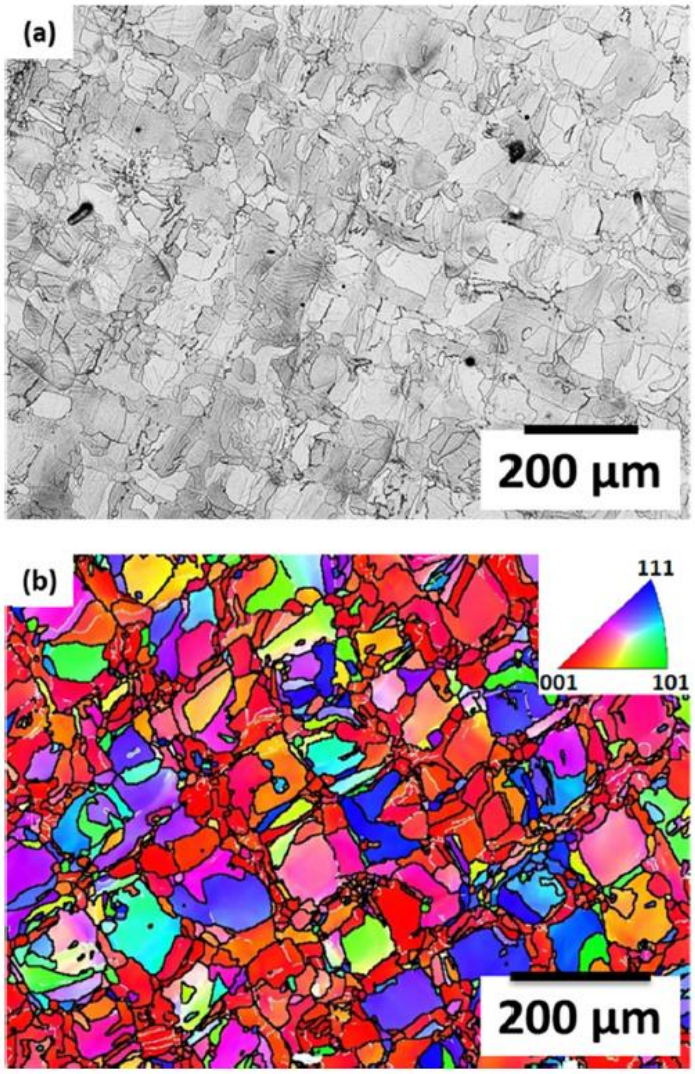

Figure 5: (a) Optical micrograph and (b) EBSD orientation map (IPF Z) of as-built 17-4 PH steel in the (X-Y) plane showing coarse grain microstructure.

In order to fully understand this observed microstructure, the metallurgical evolution of this steel was analyzed. According to the Fe-Cr-Ni alloy equilibrium phase diagram [23], this steel solidifies as primary δ-ferrite, then the ferrite fully transforms into austenite and upon further cooling the martensitic transformation occurs. However, given the relatively high cooling rates (10^5-10^6 K/s) reached by SLM process, this phase sequence is no longer valid. Several authors have investigated the solidification microstructure of stainless steels under rapid cooling. They pointed out a change in primary solidification mode from that predicted by using the ratio of the chromium equivalent to the nickel equivalent (Cr_{eq}/Ni_{eq}) [24–26]. It was found that the solidification mode not only was controlled by this ratio but also by solidification growth rate and thermal

gradient. Nonetheless, taken the SLM solidification parameters, the 17-4 PH melt pool is still predicted to solidify as 100% ferrite.

Regarding the possible transformation in the solid state, some welding investigations [27–29] on 17-4 PH steel reported an increase in the amount of retained δ ferrite with respect to the solution annealed state. They concluded that the transformation of δ ferrite to austenite was not complete because of the high cooling rates experienced during welding, which are usually in the range 10^1-10^4 K/s [30–32]. However the SLM cooling rates are 1 to 2 orders of magnitude higher than those of welding. This implies that the transformation δ ferrite → austenite γ doesn't have enough time to occur. Thus, δ (BCC) ferrite passes rapidly through the austenite (FCC) stability temperature range without transforming until reaching the stability range of the BCC phase (below ~ 600°C for this steel). No further transformation is then expected, since δ-ferrite is thermodynamically stable at low temperature. The phenomenon can be visualized as if δ ferrite had by-passed the FCC phase.

In addition, the solidified pools will encounter several thermal cycles, as illustrated in fig. 6, which is due to adjacent laser scans and the melting of upper layers. A partial re-melting of the pool upon the first subsequent layers can also occur. As shown in fig. 6, the peak temperature of the first cycles is far above the phase transformation start temperature from BCC to austenite FCC during heating (Ac1) (around ~ 600°C for this steel). Hence, the transformation might still occur. However, by taking a rate of 10^5 K/s, the maximum time spent in the FCC stability range is approximately 6 ms during heating or cooling. For kinetic reasons, this short time is supposed to be insufficient to allow austenite formation. Furthermore, according to a study [33], an increase in heating rate led to a shift of Ac1 to higher temperatures. This means that this time is even smaller than 6 ms. Moreover, a model was developed by Mondelin [34] on a similar martensitic stainless steel, which calculated the amount of transformed austenite depending on heating and cooling kinetics, by using data from dilatometric testing. Even though his model overestimated the austenitization kinetics [35], it still predicted a negligible amount of transformed austenite under SLM thermal rates (10^5-10^6 K/s). In the light of these findings, it is deduced that during these thermal cycles, either during heating or cooling, the same by-passing phenomenon is assumed to take place due to the insufficient time spent in the FCC stability range, which resulted in this observed ferritic microstructure at the end of SLM process.

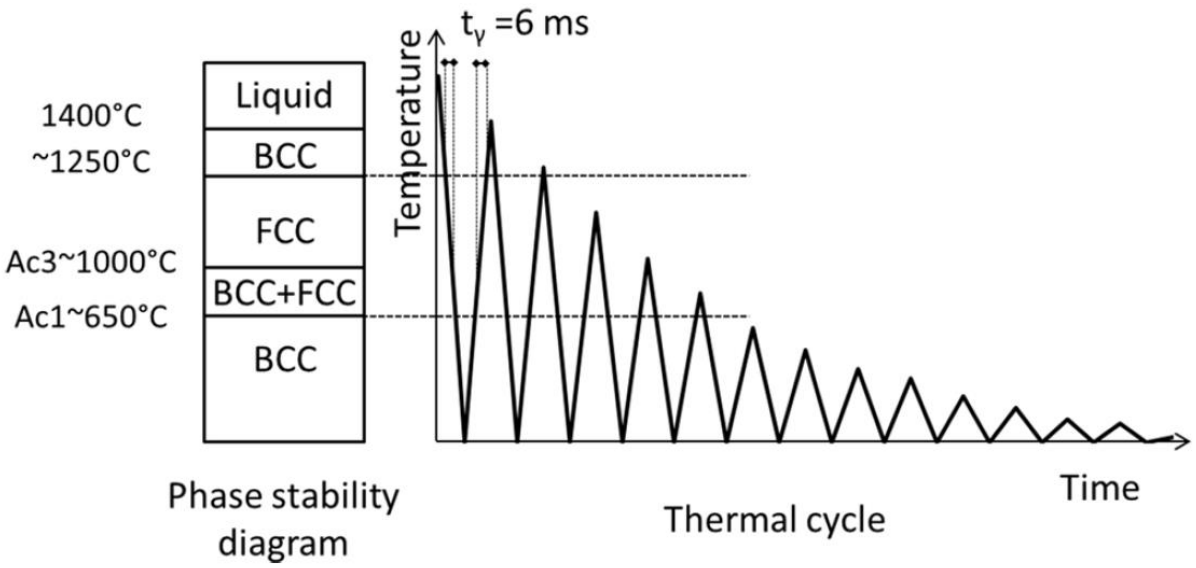

Figure 6: Schematic representation of a thermal cycle of a melt pool during SLM and the phase stability diagram of 17-4 PH steel showing that the time spent by the material in the austenite stability range is very short (6 ms), both upon cooling and heating (Ac1 and Ac3 are respectively the transformation start and finish temperatures from BCC to FCC during heating).

Furthermore, another remarkable microstructural feature related to the grain morphology can be withdrawn from the orientation maps. In fig. 4, the grains are seen elongated in the build direction following the vertical thermal gradient between the melt pool and the solidified lower layers. These columnar shaped grains can reach a length of some hundred µm, thus extending over several powder layers. This can be visualized in fig. 4(a), where the grains cross several melt pool boundaries made distinctly visible by etching. This means that during the molten pool solidification, the freshly formed crystals will have an epitaxial growth by adopting the orientation of the lower previously formed grains. It should be noted that depending on the input energy, the molten pool may include a part or the entire previous layer. Moreover in fig. 5, the plane perpendicular to build direction shows grains having a relatively geometric structure that can be associated to the laser scanning strategy. This grain morphology was also observed by K. Saeidi et al. [22] on a duplex stainless steel obtained by SLM using a similar scanning strategy and was described as a mosaic-type structure.

In order to ensure reproducibility of these results, other specimens of as-built 17-4 PH steel fabricated under argon atmosphere by different SLM machines and different powders were studied. Their orientation maps in the build direction are given in fig. 7 (a) and (b). These maps present identical microstructural characteristics to

that shown in fig. 4: the microstructure is mainly ferritic, in addition epitaxial columnar grains are observed along the build direction. These findings are remarkable, because even though these parts were fabricated by different machines and various construction parameters, or in other words have undergone different thermal histories, they all presented a ferritic microstructure. Solely the grain size and shape changed from one part to another due to different elaboration processes. At the same time there needs to be an acknowledgement that these results might not represent the general case: other types of microstructures (i.e. martensite with retained austenite) might be obtained in SLM depending on the heating/cooling rates, material composition and atmosphere. However in the three cases investigated here always the same ferritic microstructure was obtained, which at least suggests a certain generality of our conclusions.

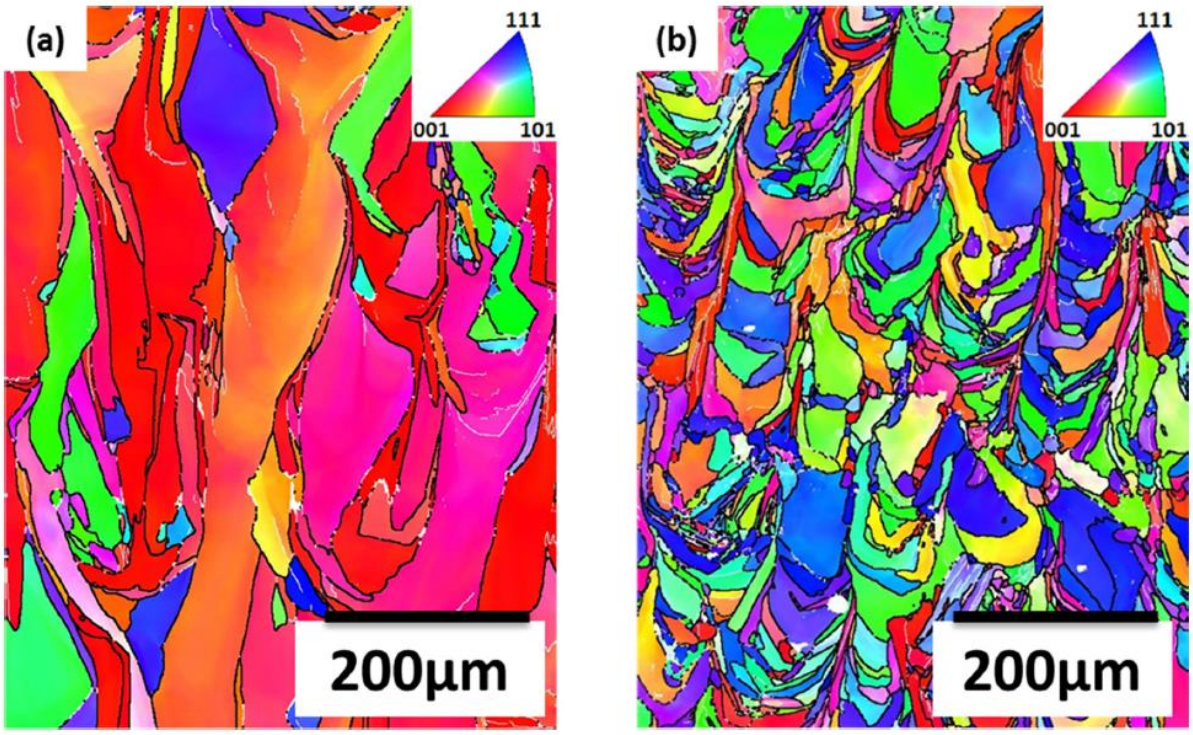

Figure 7: EBSD orientation maps (IPF Z) of as-built 17-4 PH steel in the (Y-Z) plane fabricated by (a) SLM machine 1 and (b) SLM machine 2 showing coarse grains having an epitaxial growth in the build direction. The two machines used here are different from that mainly used in this study.

Fig. 8 shows the pole figures corresponding to the (X-Y) plane of as built 17-4 PH steel shown in fig. 5. A strong fiber texture is observed with a <100> direction preferentially aligned with the build direction Z. The <100> fiber texture is the common solidification texture for cubic crystals, including FCC and BCC metals. However, steels usually undergo the phase transformation δ(BCC) → γ(FCC) → α or α'(BCC), resulting in a more random

texture [36]. Therefore, the strong fiber texture observed in fig. 8 contradicts the occurrence of this transformation sequence. In contrast, it suggests that the microstructure observed is the one obtained directly after solidification, without any further solid state phase transformation. This confirms the previous analyses that δ(BCC) phase has by-passed the austenite phase during SLM thermal cycles.

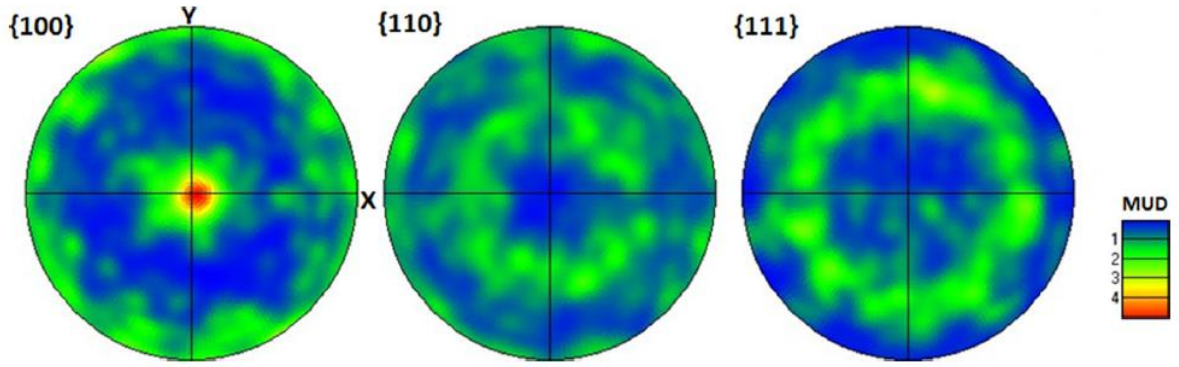

Figure 8: {100}, {110} and {111} pole figures corresponding to the (X-Y) plane of as-built 17-4 PH steel in figure 5 showing a <100> preferred orientation of grains elongated in the build direction.

Element distribution in the as-built 17-4 PH steel was investigated using EDS scans over several regions at high magnification. The colored elemental mapping images of one of these regions are given in fig. 9. Under the conditions used for EDS measurements, these maps revealed a homogeneous distribution of elements Fe, Cr, Ni, Nb, Cu and C. No precipitations of carbides or sulfides, usually found in the wrought material, were observable. Fig. 9 shows no evidence of dendrites, in contrast to some reports [18,19], where EDS measurements showed a dendritic cellular structure having a spacing of some hundreds of nm. It is well known that the solid/liquid interface morphology is mainly dependent on the solidification velocity and the temperature gradient. At very small solidification velocities, a planar interface occurs. As the velocity increases, the morphology changes to globular/cellular dendrites, then to equiaxed dendrites. At even higher growth rates, a planar front will again become stable. This phenomenon, referred to as "absolute stability" and described in details in [37–39], is characterized by diffusionless solidification and solutal trapping, resulting in a microsegregation-free structure. This explains the homogeneous distribution of elements for the as-built materials (Fig. 4(a), fig. 7(a) and (b)). It should be noted that this non-segregated microstructure can be observed only with a certain combination of process parameters that allows the solidification rates of the melt pool to exceed the critical rate for absolute stability.

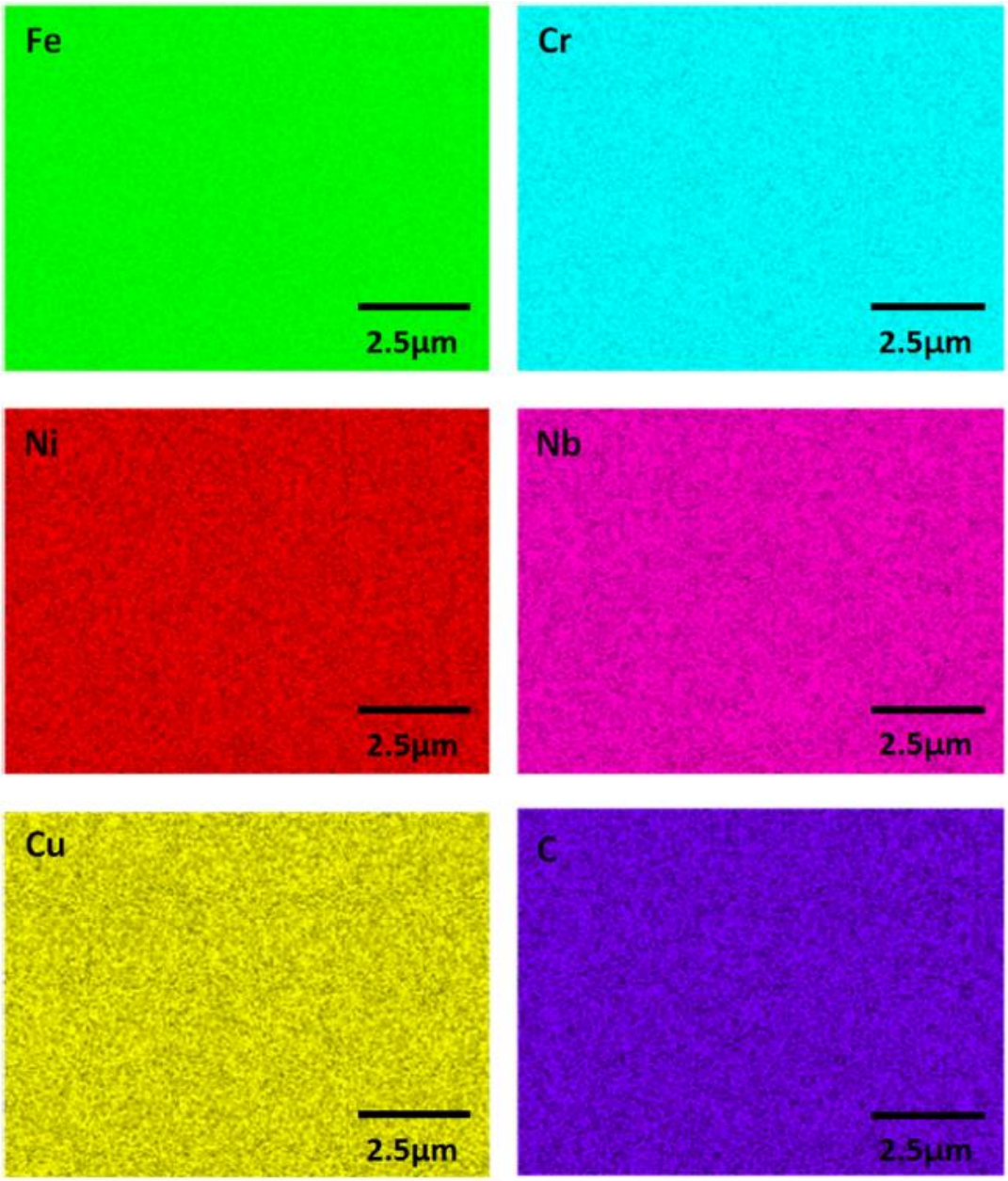

Figure 9: EDS maps of Fe, Cr, Ni, Nb, Cu and C showing a uniform distribution of elements without any segregation.

3.4. Microstructure of as-built 17-4 PH after re-austenitization heat treatment

Fig. 10 depicts the EBSD orientation map in the (Y-Z) plane of as built material after a re-austenitization treatment at 1050°C i.e. in the fully austenitic domain, followed by a quench. This heat treatment succeeded to recover the martensitic structure by allowing the steel enough time at 1050°C to austenitize. The prior austenitic grain boundaries are not clearly detectable, probably because the initial microstructure was made of very coarse grains of ferrite that can modify the austenite nucleation and growth in comparison with an initial

martensitic structure. It can also be seen that the grains exhibited a hereditary behavior by partially conserving the previous morphology of elongated grains in the (Y-Z) plane.

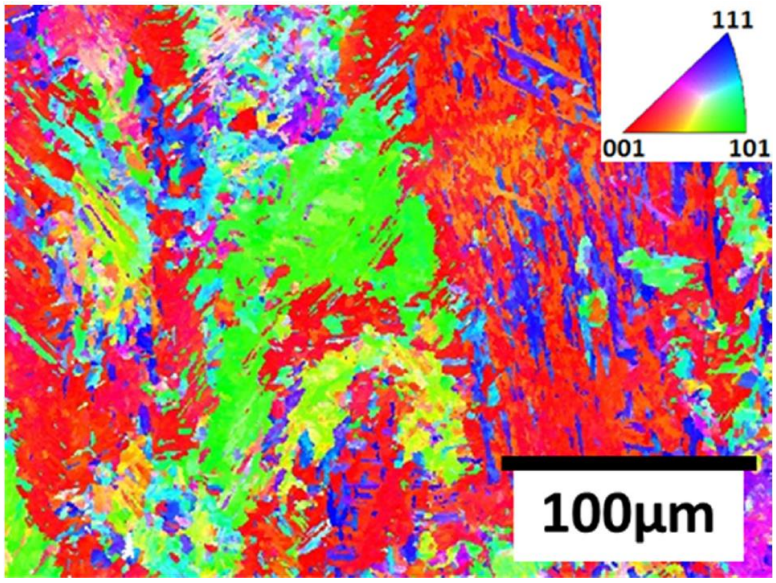

Figure 10: EBSD orientation map (IPF Z) of the (Y-Z) plane after a solution heat treatment at 1050°C and water quench showing a martensitic structure.

3.5. Dilatometric measurements

Dilatometry was performed to investigate the austenite to δ ferrite transformation at near melting temperature. The dilation curve showing the longitudinal expansion as a function of temperature is given in fig. 11. The wrought material was used for that experiment. During continuous heating, the typical transformation of martensite to austenite takes place above 600°C. Upon further heating, a deviation from linear expansion is detected around 1250°C, characterized by a volume expansion, indicating the beginning of the transformation of austenite to δ ferrite. This expansion related to γ → δ transformation is consistent with the observation conducted on pure iron [40]. As heating progressed, the curve resumed its linear behavior, proving the completion of the transformation γ → δ before reaching metal melting. In the cooling part, a straight line is observed corresponding to the fully formed ferrite shrinkage. Upon further cooling, the onset of the reverse transformation δ → γ occurs, identified by a deviation from this line. The austenite is then fully formed and is stable, or metastable, until ~ 130°C, where it undergoes the usual diffusionless martensitic transformation. This

dilatometric measurement is an indication that 17-4 PH stainless steel is fully ferritic at high temperatures (above ~ 1320°C).

Another dilatomtric test was carried out on as-built SLM-ed 17-4 PH steel to examine its transformation behavior. The initial state of this material is δ ferrite. Fig. 12 depicts the curve of dilation as a function of temperature. During heating, δ ferrite transformed normally to austenite. During cooling, the austenite to martensite transformation occurred. The identical behavior of δ ferrite and martensite regarding the phase transformation to austenite is not surprising since both phases have the same BCC structure. This result is consistent with the microstructural observation of as-built 17-4 PH steel after solution heat treatment (fig. 10), showing that the martensitic microstructure can be recovered from the ferritic as-built material after heat treatment at 1050°C , followed by quenching.

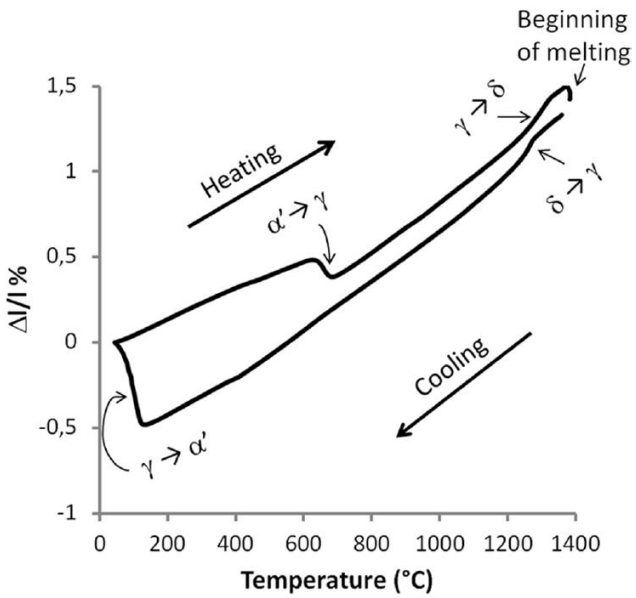

Figure 11: Dilation as a function of temperature for 17-4 PH steel showing the formation of δ ferrite above 1250°C. The material used for this experiment was the conventional 17-4 PH steel.

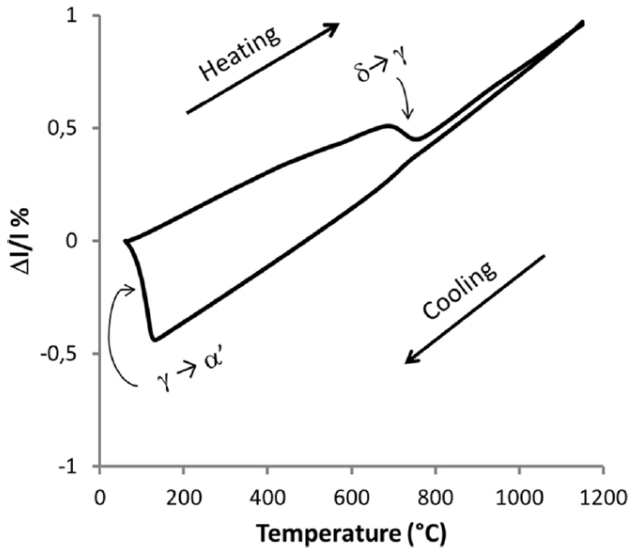

Figure 12: Dilation as a function of temperature for as-built SLM-ed 17-4 PH steel showing a complete austenitization during heating and the martensitic transformation upon cooling. The initial state of the material is δ ferrite.

4. Conclusion

In this study, microstructural characterization was conducted on 17-4 PH steel in the as-built state produced by SLM. Several conclusions can be made about the observed microstructure:

1. Due to the high cooling and heating rates reached during SLM (10^5-10^6 K/s), the austenite phase doesn't have enough time to be formed. This means that the 17-4 PH steel, after solidification in δ ferrite, encounters no further metallurgic transformation during its thermal cycles. This results in a stable ferritic microstructure at the end of the SLM process.
2. The large thermal gradient existing between the melt pool and the previously solidified layers promoted a highly anisotropic microstructure having coarse grains elongated along the build direction. In addition, these grains are seen to cross several layers suggesting the occurrence of an epitaxial solidification.

3. A strong fiber texture was observed with the <100> crystal orientation aligned preferentially with the build direction. The conservation of this solidification texture contradicts the possible existence of any phase transformation in the solid state during the process.

4. A diffusionless solidification can be concluded from the EDS results that showed a homogeneous distribution of alloying elements inside the grains. Due to the high cooling rates, the planar solid/liquid interface was stabilized ("absolute stability") resulting in a diffusion free solidification with solute trapping and a segregation-free microstructure.

5. Other specimens of as-built 17-4 PH steel fabricated in different SLM machines were also studied. Despite their variable process parameters that produced different thermal histories for each piece, they all had similar microstructural characteristics. The high thermal rates produced the same ferritic structure.

5. References

[1] N. Guo, M.C. Leu, Additive manufacturing: technology, applications and research needs, Frontiers of Mechanical Engineering. 8 (2013) 215–243. doi:10.1007/s11465-013-0248-8.

[2] J.-P. Kruth, M.-C. Leu, T. Nakagawa, Progress in additive manufacturing and rapid prototyping, Cirp Annals. 47 (1998) 525–540. doi:10.1016/S0007-8506(07)63240-5.

[3] L.E. Murr, E. Martinez, K.N. Amato, S.M. Gaytan, J. Hernandez, D.A. Ramirez, P.W. Shindo, F. Medina, R.B. Wicker, Fabrication of Metal and Alloy Components by Additive Manufacturing: Examples of 3D Materials Science, Journal of Materials Research and Technology. 1 (2012) 42–54. doi:10.1016/S2238-7854(12)70009-1.

[4] M. Rombouts, J.-P. Kruth, L. Froyen, P. Mercelis, Fundamentals of selective laser melting of alloyed steel powders, CIRP Annals-Manufacturing Technology. 55 (2006) 187–192. doi:10.1016/S0007-8506(07)60395-3.

[5] J.P. Kruth, L. Froyen, J. Van Vaerenbergh, P. Mercelis, M. Rombouts, B. Lauwers, Selective laser melting of iron-based powder, Journal of Materials Processing Technology. 149 (2004) 616–622. doi:10.1016/j.jmatprotec.2003.11.051.

[6] A.V. Gusarov, I. Yadroitsev, P. Bertrand, I. Smurov, Heat transfer modelling and stability analysis of selective laser melting, Applied Surface Science. 254 (2007) 975–979. doi:10.1016/j.apsusc.2007.08.074.

[7] M. Averyanova, E. Cicala, P. Bertrand, D. Grevey, Experimental design approach to optimize selective laser melting of martensitic 17-4 PH powder: part I-single laser tracks and first layer, Rapid Prototyping Journal. 18 (2012) 28–37. doi:10.1108/13552541211193476.

[8] T. Niendorf, S. Leuders, A. Riemer, H.A. Richard, T. Tröster, D. Schwarze, Highly Anisotropic Steel Processed by Selective Laser Melting, Metallurgical and Materials Transactions B. 44 (2013) 794–796. doi:10.1007/s11663-013-9875-z.

[9] S. Dadbakhsh, B. Vrancken, J.-P. Kruth, J. Luyten, J. Van Humbeeck, Texture and anisotropy in selective laser melting of NiTi alloy, Materials Science and Engineering: A. 650 (2016) 225–232. doi:10.1016/j.msea.2015.10.032.

[10] U.K. Viswanathan, S. Banerjee, R. Krishnan, Effects of aging on the microstructure of 17-4 PH stainless steel, Materials Science and Engineering: A. 104 (1988) 181–189. doi:10.1016/0025-5416(88)90420-X.

[11] W.D. Yoo, J.H. Lee, K.T. Youn, Y.M. Rhyim, Study on the Microstructure and Mechanical Properties of 17-4 PH Stainless Steel Depending on Heat Treatment and Aging Time, Solid State Phenomena. 118 (2006) 15–20. doi:10.4028/www.scientific.net/SSP.118.15.

[12] C.N. Hsiao, C.S. Chiou, J.R. Yang, Aging reactions in a 17-4 PH stainless steel, Materials Chemistry and Physics. 74 (2002) 134–142. doi:10.1016/S0254-0584(01)00460-6.

[13] Z. Hu, H. Zhu, H. Zhang, X. Zeng, Experimental investigation on selective laser melting of 17-4PH stainless steel, Optics & Laser Technology. 87 (2017) 17–25. doi:10.1016/j.optlastec.2016.07.012.

[14] A. Yadollahi, N. Shamsaei, S.M. Thompson, A. Elwany, L. Bian, Effects of building orientation and heat treatment on fatigue behavior of selective laser melted 17-4 PH stainless steel, International Journal of Fatigue. 94 (2017) 218–235. doi:10.1016/j.ijfatigue.2016.03.014.

[15] A. Yadollahi, N. Shamsaei, S.M. Thompson, A. Elwany, L. Bian, Mechanical and microstructural properties of selective laser melted 17-4 PH stainless steel, in: ASME 2015 International Mechanical Engineering Congress and Exposition, American Society of Mechanical Engineers, 2015: p. V02AT02A014–V02AT02A014. http://proceedings.asmedigitalcollection.asme.org/proceeding.aspx?articleid=2500381 (accessed October 27, 2016).

[16] L.E. Murr, E. Martinez, J. Hernandez, S. Collins, K.N. Amato, S.M. Gaytan, P.W. Shindo, Microstructures and properties of 17-4 PH stainless steel fabricated by selective laser melting, Journal of Materials Research and Technology. 1 (2012) 167–177. doi:10.1016/S2238-7854(12)70029-7.
[17] T. LeBrun, T. Nakamoto, K. Horikawa, H. Kobayashi, Effect of retained austenite on subsequent thermal processing and resultant mechanical properties of selective laser melted 17–4 PH stainless steel, Materials & Design. 81 (2015) 44–53. doi:10.1016/j.matdes.2015.05.026.
[18] H.K. Rafi, D. Pal, N. Patil, T.L. Starr, B.E. Stucker, Microstructure and Mechanical Behavior of 17-4 Precipitation Hardenable Steel Processed by Selective Laser Melting, Journal of Materials Engineering and Performance. 23 (2014) 4421–4428. doi:10.1007/s11665-014-1226-y.
[19] S. Cheruvathur, E.A. Lass, C.E. Campbell, Additive Manufacturing of 17-4 PH Stainless Steel: Post-processing Heat Treatment to Achieve Uniform Reproducible Microstructure, JOM. 68 (2016) 930–942. doi:10.1007/s11837-015-1754-4.
[20] P. Lacombe, B. Baroux, G. Béranger, in: Les aciers inoxydables, Ed. de physique, Les Ulis, 1991: p. 496.
[21] F. Hengsbach, P. Koppa, K. Duschik, M.J. Holzweissig, M. Burns, J. Nellesen, W. Tillmann, T. Tröster, K.-P. Hoyer, M. Schaper, Duplex stainless steel fabricated by selective laser melting - Microstructural and mechanical properties, Materials & Design. 133 (2017) 136–142. doi:10.1016/j.matdes.2017.07.046.
[22] K. Saeidi, L. Kevetkova, F. Lofaj, Z. Shen, Novel ferritic stainless steel formed by laser melting from duplex stainless steel powder with advanced mechanical properties and high ductility, Materials Science and Engineering: A. 665 (2016) 59–65. doi:10.1016/j.msea.2016.04.027.
[23] D. Peckner, I.M. Bernstein, eds., in: Handbook of Stainless Steels, McGraw-Hill, New York, 1977: p. 4.11.
[24] J.C. Lippold, D.J. Kotecki, in: Welding Metallurgy and Weldability of Stainless Steels, John Wiley, Hoboken, NJ, 2005: pp. 264–286.
[25] S. Fukumoto, W. Kurz, Solidification Phase and Microstructure Selection Maps for Fe-Cr-Ni Alloys., ISIJ International. 39 (1999) 1270–1279. doi:10.2355/isijinternational.39.1270.
[26] E. Johnson, L. Grabak, A. Johansen, L.S. Kristensen, J.V. Wood, Microstructure of rapidly solidified stainless steel, Materials Science and Engineering. 98 (1988) 301–303. doi:10.1016/0025-5416(88)90174-7.
[27] C.R. Das, H.C. Dey, G. Srinivasan, S.K. Albert, A.K. Bhaduri, A. Dasgupta, Weldability of 17-4PH stainless steel in overaged heat treated condition, Science and Technology of Welding and Joining. 11 (2006) 502–508. doi:10.1179/174329306X148147.
[28] W. Liu, J. Ma, M.M. Atabaki, R. Pillai, B. Kumar, U. Vasudevan, H. Sreshta, R. Kovacevic, Hybrid Laser-arc Welding of 17-4 PH Martensitic Stainless Steel, Lasers in Manufacturing and Materials Processing. 2 (2015) 74–90. doi:10.1007/s40516-015-0007-2.
[29] A. Ziewiec, A. ZieliŃska-Lipiec, E. Tasak, Microstructure of Welded Joints of X5CrNiCuNb16-4 (17-4 PH) Martensitic Stainlees Steel After Heat Treatment, Archives of Metallurgy and Materials. 59 (2014). doi:10.2478/amm-2014-0162.
[30] J.W. Elmer, The influence of cooling rate on the microstructure of stainless steel alloys, 1988. doi:10.2172/5678406.
[31] G. Turichin, M. Kuznetsov, M. Sokolov, A. Salminen, Hybrid Laser Arc Welding of X80 Steel: Influence of Welding Speed and Preheating on the Microstructure and Mechanical Properties, Physics Procedia. 78 (2015) 35–44. doi:10.1016/j.phpro.2015.11.015.
[32] K. Poorhaydari, B.M. Patchett, D.G. Ivey, Estimation of Cooling Rate in the Welding of Plates with Intermediate Thickness, Welding Journal. 84 (2005) 149s-155s.
[33] R. Kapoor, I.S. Batra, On the α′ to γ transformation in maraging (grade 350), PH 13-8 Mo and 17-4 PH steels, Materials Science and Engineering: A. 371 (2004) 324–334. doi:10.1016/j.msea.2003.12.023.
[34] A. Mondelin, Modélisation de l'intégrité des surfaces usinées: Application au cas du tournage finition de l'acier inoxydable 15-5PH, Ecole Centrale de Lyon, 2012. https://tel.archives-ouvertes.fr/tel-00838512/ (accessed August 30, 2017).
[35] F. Christien, M.T.F. Telling, K.S. Knight, A comparison of dilatometry and in-situ neutron diffraction in tracking bulk phase transformations in a martensitic stainless steel, Materials Characterization. 82 (2013) 50–57. doi:10.1016/j.matchar.2013.05.002.
[36] S. Suwas, R.K. Ray, in: Crystallographic Texture of Materials, Springer London, London, 2014: pp. 73–88. doi:10.1007/978-1-4471-6314-5.
[37] Doru M. Stefanescu, Roxana Ruxanda, Fundamentals of Solidification, ASM International. 9 (2004) 71–92.
[38] W. Kurz, D.J. Fisher, in: Fundamentals of Solidification, 3rd ed., Trans Tech Publications, 1992: pp. 133–161.
[39] M.E. Glicksman, in: Principles of Solidification, Springer New York, New York, NY, 2011: pp. 427–446. doi:10.1007/978-1-4419-7344-3.
[40] Z.S. Basinski, W. Hume-Rothery, A.L. Sutton, The Lattice Expansion of Iron, Proceedings of the Royal Society A: Mathematical, Physical and Engineering Sciences. 229 (1955) 459–467. doi:10.1098/rspa.1955.0102.

List of figures:

Figure 1: Schematic representation of the build orientation and the planes at which the microstructural characterization was carried out.

Figure 2: (a) Optical micrograph and (b) EBSD orientation map (IPF Z) of wrought 17-4 PH steel showing a typical martensitic microstructure with a mean grain size of 18 μm.

Figure 3: XRD patterns of as-built 17-4 PH steel (a) in the (Y-Z) plane parallel to the build direction and (b) in the (X-Y) plane perpendicular to the build direction.

Figure 4: (a) Optical micrograph and (b) EBSD orientation map (IPF Z) of as-built 17-4 PH steel in the (Y-Z) plane showing coarse grains with epitaxial growth in the build direction.

Figure 5: (a) Optical micrograph and (b) EBSD orientation map (IPF Z) of as-built 17-4 PH steel in the (X-Y) plane showing coarse grain microstructure.

Figure 6: Schematic representation of a thermal cycle of a melt pool during SLM and the phase stability diagram of 17-4 PH steel showing that the time spent by the material in the austenite stability range is very short (6ms), both upon cooling and heating.

Figure 7: : EBSD orientation maps (IPF Z) of as-built 17-4 PH steel in the (Y-Z) plane fabricated by (a) SLM machine 1 and (b) SLM machine 2 showing coarse grains having an epitaxial growth in the build direction. The two machines used here are different from that mainly used in this study.

Figure 8: {100}, {110} and {111} pole figures corresponding to the (X-Y) plane of as-built 17-4 PH steel in figure 5 showing a <100> preferred orientation of grains elongated in the build direction.

Figure 9: EDS maps of Fe, Cr, Ni, Nb, Cu and C showing a uniform distribution of elements without any segregation.

Figure 10: EBSD orientation map (IPF Z) of the (Y-Z) plane after a solution heat treatment at 1050°C and water quench showing a martensitic structure.

Figure 11: Dilation as a function of temperature for 17-4 PH steel showing the formation of δ ferrite above 1250°C. The material used for this experiment was the conventional 17-4 PH steel.

Figure 12: Dilation as a function of temperature for as-built SLM-ed 17-4 PH steel showing a complete austenitization during heating and the martensitic transformation upon cooling. The initial state of the material is δ ferrite.